EL NINO EPISODE—RELATED NH 100 hPa CIRCULATION ANOMALY①

Shi Neng (施 能), Shen Tongli (沈桐立)

Nanjing Institute of Meteorology, Nanjing 210044

and Cao Hongxing (曹鸿兴)

China Academy of Meteorological Sciences, Beijing 100081

Received 14 December 1993; accepted 28 April 1994

ABSTRACT

Investigation is carried out of winter Northern Hemisphere (NH) 100 hPa teleconnection, indicating the existence of a PNA pattern whose wavetrain well resembles that at 500 hPa level. During the climax of the El Nino episode (winter), the 100 PNA becomes strong, a fact that manifests itself more clearly than at the 500 hPa level. Moreover, study is made of the anomaly in the tropical monthly windfield and mean circulation on a seasonal basis in a range of phases of the El Nino event. Results show that the 100 hPa geopotential height is lowered on a large scale in the spring and previous winter with the event happening as compared to a La Nina year, wherewith diagnosis is performed of the 1991/1992 El Nino episode.

Key words: 100 hPa height, PNA teleconnection pattern, El Nino event, circulation anomaly, intensity index

I. INTRODUCTION

Now still of particular interest for meteorologists and oceanologists are El Nino episodes and the related feeble Southern Oscillation (ENSO) genesis and development. ENSO is known to bear relation to the anomaly of atmospheric circulations and weather/climate on a global basis. Following Wallace and Gutzler (1981)who reported their finding of winter Northern Hemisphere teleconnection patterns, much work has been directed towards their relation to ENSO (Shukla and Wallace, 1983; Hoskins and Karoly, 1981). In their analysis of the nearly 40-year record on the Northern Hemisphere circulation, Zhu and Shi (1992) showed that at the peak of the El Nino event in winter, the most pronounced anomaly at 500 hPa is a highly feeble WP pattern, predominant over a vigorous PNA pattern and that the teleconnections produced anomaly response during the El Nino genesis and development. A Shi-Cao three-level discriminant model (1992), which is based on 500-hPa teleconnection intensity and Southern Oscillation indices and

① This study is supported in part by China SMA's Project of Theory and Method for Short—Range Climatic Prediction and in part by China Foundation for Meteorological Institutions.

capable of diagnosing in August if the event has occurred in the preceding period, has shown positive result in tests against the nearly 40-year El Nino record. El Nino-associated 700-and 200-hPa circulation anomaly was reported by Chen (1982) and Arkin (1982). By comparison, our article presents a quantitative study on the relation of 100 hPa PNA intensity to the El Nino episode and on the anomaly features of 100 hPa seasonal circulation and low-latitude monthly zonal wind in the El Nino year before a scheme is developed with these analyses to diagnose and predict episodes to come.

Ⅱ. WINTER NORTHERN HEMISPHERE 100 hPa TELECONNECTION IN RELATION TO EL NINO

1. *Data and method*

A winter mean map is prepared in the context of Northern Hemisphere 1956/57—1989/90 DJF monthly gridded data at 100 hPa with 36 meridional (10°E—0°) and 8 zonal (10—80°N) grid points, totalling in 288 points globally. Then the Wallace's algorithm is employed to calculate the teleconnection coefficient

$$r_i = |\min_j(r_{ij})| \qquad i = 1,2,\cdots,288; \quad j = 1,2,\cdots,288; \quad i \neq j$$

Pairs of maxima of r_i derived constitute a teleconnection structure. Calculations show that at 100 hPa level there also exists such a structure in the central Pacific that follows a great circle route toward the north and then turns southeastward, reaching North America. Following Wallace's definition of the 500 hPa teleconnection, the 100 hPa PNA intensity index (II in short) is given as

$$\mathrm{PNA(100\ hPa)} = \frac{1}{4}H^*(20°\mathrm{N},180°\mathrm{E}) - \frac{1}{2}H^*(50°\mathrm{N},170°\mathrm{W}) + \frac{1}{4}H^*(60°\mathrm{N},110°\mathrm{W})$$

and the 500 hPa II has the form

$$\mathrm{PNA(500\ hPa)} = \frac{1}{4}[H^*(20°\mathrm{N},160°\mathrm{W}) - H^*(45°\mathrm{N},165°\mathrm{W}) + H^*(55°\mathrm{N},115°\mathrm{W}) - H^*(30°\mathrm{N},85°\mathrm{W})]$$

Fig. 1 is a diagram of one-point correlation with the reference point at 50°N, 170°W, where the contours ranging from 0.90—0.70 are spaced at 0.1, with dotted lines denoting negative values and heavy solid (great arc) the centrioid of the 500 (100) hPa PNA's.

2. *Winter* 100 hPa PNA *in relation to* El Nino *episode*

The winter 100 hPa PNA IIs coming from the above definition are summarized in the left-hand column of each portion of Table 1, with the 500 hPa values taken from Zhu and Shi (1992). The E (L_a) represents the start of the El Nino (La Nina) year. Note that some authors had 1984 specified as a La Nina episode, which does not affect our computations.

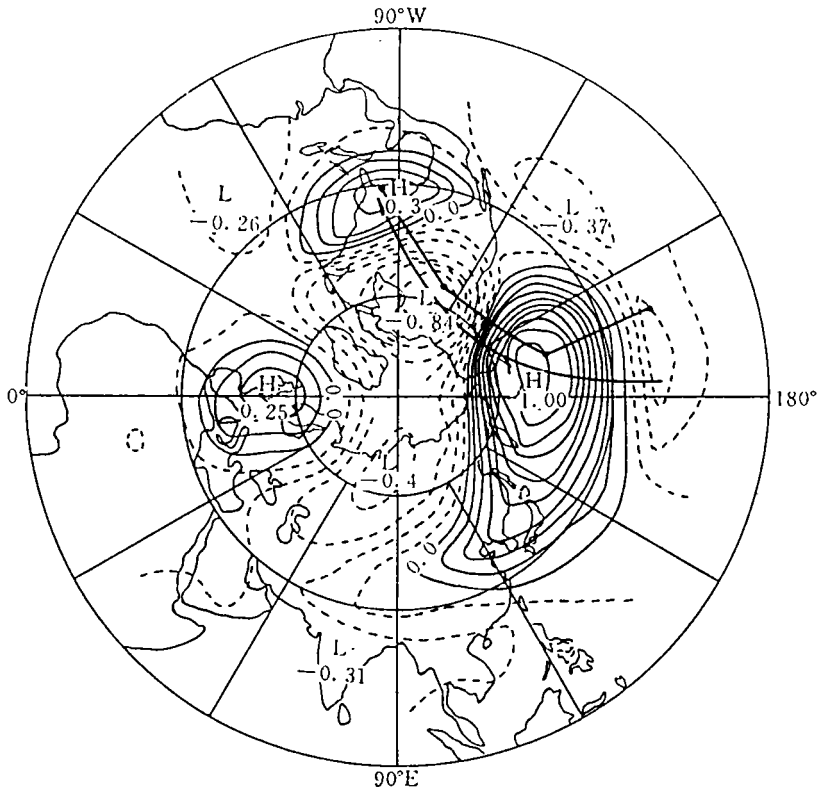

Fig. 1. A plot of winter 100 hPa one-point correlations with the reference point at 50°N, 170°W.

Based on Table 1, a correlation coefficient of 0.87 is obtained for the 1956—1990 PNA IIs at 100 and 500 hPa levels, showing the closeness in the intensity and location of the PNA patterns between the two levels both having barotropicity. Viewed from the relation to El Nino events, however, the 100 hPa PNAs are more closely associated with the events than the 500 hPa analogs. The t statistic test used is in the form of

$$t = (\bar{x}_1 - \bar{x}_2) \Big/ \left(\frac{n_1\sigma_1^2 + n_2\sigma_2^2}{n_1 + n_2 - 2} \cdot \frac{1}{n_1} + \frac{1}{n_2} \right)^{\frac{1}{2}}$$

where n_0 (n_2) denotes the year of El Nino (La Nina), x_1 (x_2) and σ_1 (σ_2) the PNA II mean and mean square deviation, respectively, in the El Nino (La Nina) year. With the aid of the above expression, t is calculated for 100 and 500 hPa, separately, in terms of 1956—1990 data, resulting in

$$t(100\ \text{hPa}) = 4.627, \qquad t(500\ \text{hPa}) = 3.151.$$

The 100 hPa significance attains 0.005 compared to 0.01 for the 500 hPa t value, sug-

gesting that the intensity in the PNA is higher at 100 hPa than at 500 hPa in winter associated with an El Nino episode. As found in the record studied, the 100-hPa PNA IIs are never lower than −0.05 (1968) whereas many of the 500-hPa cases are weak PNA patterns, e. g., −0.84 (1951), −0.33 (1953), −0.59 (1968) and −0.21 (1965).

Table 1. Winter 100-and 500-hPa PNA IIs and low-latitude westerly indices (U−I) in relation to El Nino or La Nina episodes.

Year	PNA I		E/L_a	UI		Year	PNA I		E/L_a	UI	
				Oct.	Jun.					Oct.	Jun.
	100 hPa	500 hPa		100—120°E	170—160°W		100 hPa	500 hPa		100—120°E	170—160°W
1951	—	−0.84	E			1971	−4.26	−1.20		−3.0	5.0
1952	—	−0.33				1972	0.54	0.09	E	3.5	9.0
1953	—	−0.33	E			1973	−1.70	−0.26	L_a	−4.5	−6.0
1954	—	−0.61	L_a			1974	0.93	−0.11		−3.5	10.5
1955	—	−0.97	L_a			1975	−0.84	−0.12	L_a	−11.5	2.0
1956	−3.94	−1.15		11.0	−1.5	1976	2.96	1.21	E	0.0	12.0
1957	1.35	0.79	E	15.5	7.0	1977	1.10	0.81		5.5	11.5
1958	0.37	−0.17		3.5	7.5	1978	−1.40	−0.48		0.0	4.0
1959	1.76	0.55		−0.5	4.0	1979	0.04	0.34		16.0	8.5
1960	1.65	0.64		−1.0	2.5	1980	1.79	0.76		0.0	11.0
1961	−1.90	−0.31		0.5	−4.0	1981	−1.26	−0.56		−4.5	3.0
1962	−0.79	0.38		−2.0	7.0	1982	2.07	0.94	E	0.5	5.0
1963	0.56	0.72	E	17.0	5.0	1983	−0.68	0.22		−10.5	6.5
1964	−3.00	−0.71	L_a	−15.0	1.0	1984	−1.67	−0.29		−12.5	2.0
1965	0.12	−0.21	E	10.0	−1.0	1985	0.95	0.88		−7.5	2.5
1966	−0.05	0.06		11.5	7.5	1986	3.21	0.86	E	5.5	6.0
1967	−0.81	−0.10	L_a	−0.5	3.5	1987	2.02	0.33		−5.5	5.5
1968	−0.05	−0.59	E	−1.5	2.5	1988	−1.65	−0.66	L_a	−16.5	−3.5
1969	3.94	0.66		14.0	5.5	1989	−0.56	−0.21		−7.0	0
1970	−0.75	−0.56	L_a	−1.0	3.0	1990	0.21	−0.11		−1.5	1.5
						1991	1.47	−0.23	E	4.5	5.0

Ⅲ. RELATION OF ANOMALY IN 100 hPa TROPICAL WIND FIELD TO EL NINO EPISODE

1. *Spatial/temporal variation in* 100 hPa *low-latitude wind in relation to* El Nino *episode*

Because of lack of complete dataset of tropical wind, the 100 hPa monthly height difference (15°N minus 25°N) is employed which is normally proportional to the westerly value over the belt at the same level, or 100 hPa low-latitude westerly intensity index, denoted as UI.

Fig. 2a depicts the difference (El Nino minus La Nina) based on monthly mean UI from the data of 8 and 6 years with the former and latter starting , respectively (refer to Table 1). There the single-and double-lined areas stand for the difference of 2.0 and 3.0, respectively, and the blackened area is one that exceeds 4.0, with the dotted line

denoting a negative value. To verify the difference significance, we present Mahalanobis squared distance (Fig. 2b) by means of the magnitudes of Fig. 2a. As shown in Fig. 2b, the contour begins with 1.0, with the interval of 1.0. Following statistical test theory, for the degree of freedom of 12, the squared distance of > 1.38 arrives at the significance of 0.05 and > 2.722 of 0.01. However, the vigorous anomaly occurs in

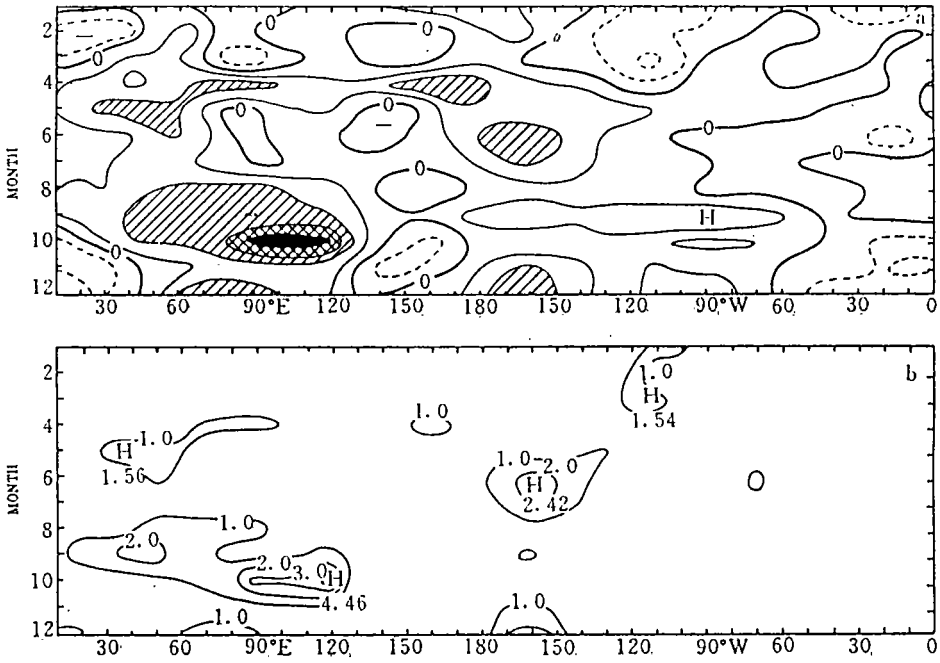

Fig. 2. Composite chart of monthly 100 hPa height difference (El Nino−La Nina, in units of dam) between 15 and 25°N (a) and the related Mahalanobis squared distance test (b).

i) 15−25°N, 90−120°E in the period September to October, which covers the Bay of Bengal to the South China Sea to Taiwan in the El Nino year ; the September − October 100−120°E mean UI given in Table 1 indicates pronounced difference between the El Nino and La Nina years; and in

ii) 15−25°N, 180−150°W in June through July, which is in the central Pacific and the period is the time of El Nino burgeoning and of 100 hPa westerly strengthening. The June 170−160°W averaged UI on the left side of the table indicates that, during the El Nino episode, the eastern Pacific SST rises, leading to the invigorated Hadley circulation that plays an important role in transporting westerly angular momentum into higher levels and then northward. Our work demonstrates that the westerly intensification in

June—July occurs mainly in the central Pacific and that as autumn comes, over the Indian Ocean and western Pacific.

2. 100 hPa *longitudinal height difference in various latitute belts over* 100—120°E *in association with* El Nino *events*

As stated earlier, the 100—120°E tropical westerly is greatly enhanced in October in the El Nino year. Now consider other latitude belts. For this purpose a cross section is constructed (Fig. 3). Then, significance test is made of the longitudinal geopotential height difference of a range of latitude bands. Tests show that the significance of 0.001 is reached only in such belts as 40—50°N, 20—30°N and 15—25°N (as asterisked in Fig. 3) with the t statistic of 6.53, 5.93 and 4.15, respectively. All these show that in October of the episode, 100 hPa westerly is considerably diminished over 40—50°N, 100—120°E and will be enhanced at low latitudes. The direct cause of the change in the windfields lies in that geopotential height is appreciably lowered over Korea and the Sea of Japan and raised over tropical latitudes in this season. This will be further dealt with in Section Ⅳ.

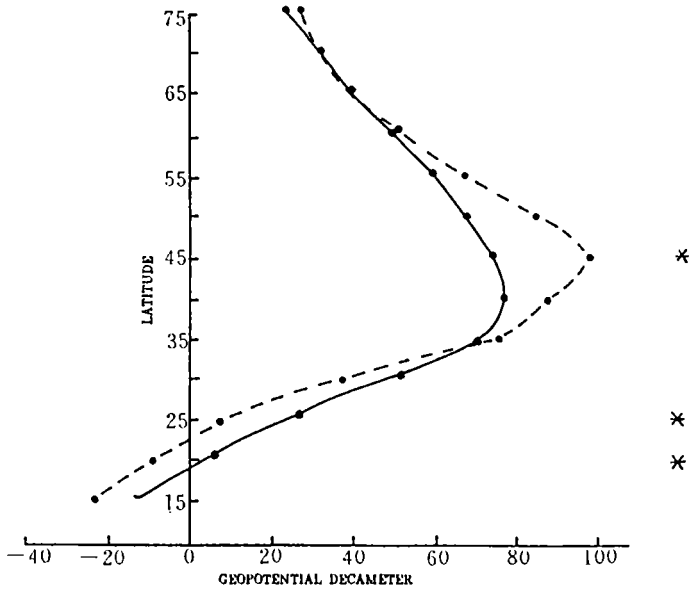

Fig. 3. 100—120°E mean longitudinal difference (15° minus 25°) at 100 hPa level in October. The solid line denotes the El Nino and the dashed La Nina event.

Ⅳ. 100 hPa SEASONAL MEAN CIRCULATION ANOMALY BEFORE AND AFTER THE EPISODE

Using the monthly 100 hPa mean the seasonal averages are derived for each of the gridpoints in every 3 months of spring (MAM), summer (JJA), autumn (SON) and winter (DJF), followed by composition of the seasonal maps with the El Nino and La Nina years, wherewith the differences (El Nino minus La Nina) are calculated. In order to remove the problem with non-uniformity in gridpoint variance, the difference for each point on the map is divided by its corresponding seasonal mean square deviation (MSD), which can be realized in virtue of

$$t_{it} = \frac{\overline{H}_{1it} - \overline{H}_{2it}}{\sigma_{it}}$$

where $i = 1, 2, \ldots, 288$ (gridpoints); $t = 1, 2, 3, 4$ (seasons); subscript 1 (2) represents the El Nino (La Nina) year; H stands for the 100 hPa seasonal height with the overbar denoting the mean. Analogous to t statistic, this expression can be statistically tested in terms of t distribution. Fig. 4 presents a MSD-normalized difference chart (t) where the dashed line gives a negative value and contours are spaced at 0.3. One can see from Fig. 4 the detailed features of the seasonal difference on a seasonal basis as follows.

(1) Spring (MAM)

This season is the period of El Nino burgeoning, indicated in Fig. 4 by negative values of an overwhelming majority of t, i.e., 271 in 288 gridpoints show negative magnitudes, with a limited area of positive values displayed only around the Kamchatka Pen. and a strong negative value (-1.48) shows up in the central Pacific and another one (-1.54) slightly westward of Iceland. It is worthwhile to make an approach to the mechanism for the lowered large-scale 100-hPa geopotential height in the El Nino year as opposed to the case in the La Nina episode. It is found that, of the 288 gridpoints, 188 have negative values by comparing the values of an El Nino year to long term mean.

(2) Summer (JJA)

The summer difference map exhibits a large-scale negative region, indicating a lower 100 hPa height in the El Nino than in the La Nina year. Calculations show that 242 out of the 288 gridpoints have negative values. There appears a faint polar positve region and another positive sector is emerging in the central Pacific at low latitudes and expected to expand and invigorate. Comparison of the El-Nino-year average with long-term mean for the 100 hPa yields a similar result to the above except that the area of negative values is decreased a little, with negative anomaly in 163 of the 288 gridpoints.

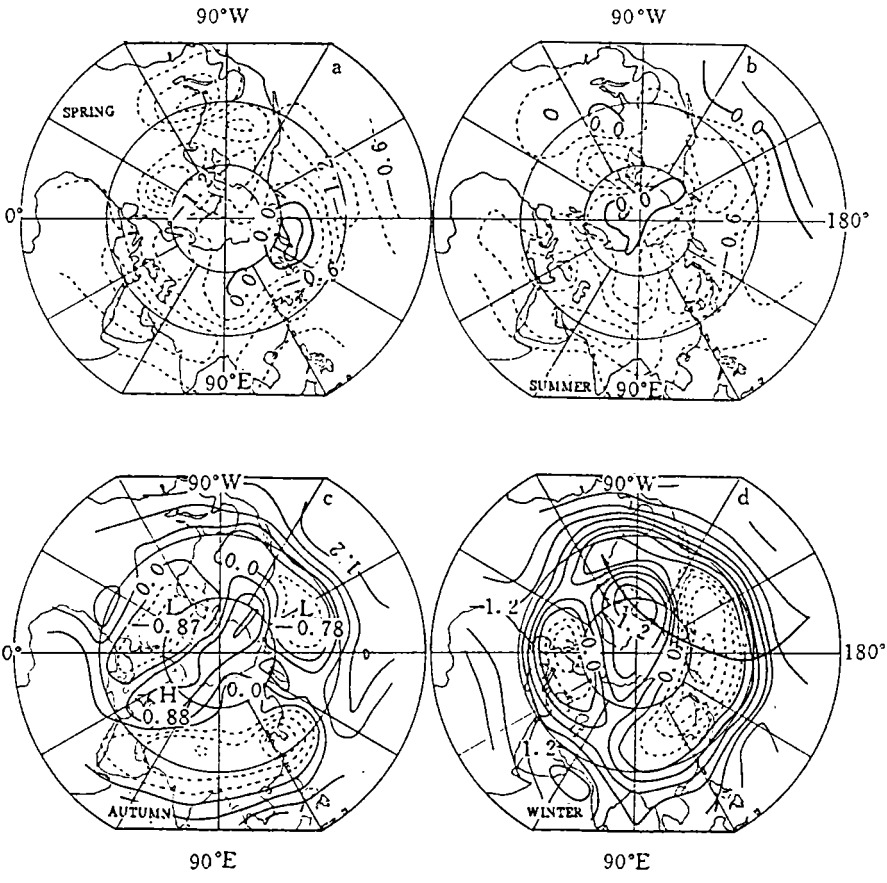

Fig. 4. The MSD-normalized difference (El Nino minus La Nina) at 100 hPa level on a seasonal basis. Spring (a), summer (b), fall (c) and winter (d).

(3) Autumn (SON)

The El Nino is clearly manifested in this season. The summer positive t belt in the central Pacific has considerably enlarged on both sides so that a large-scale positive band covers the tropical waters as a whole (Fig. 4c), with a maximum of 1.34 in the core (10°N, 150°W). Additionally, a negative center (−1.39) in the Sea of Japan (40°N, 110—130°E) is responsible for the enfeebled 100-hPa westerly (40—50°N, 100—120°E) during the El Nino episode, a result that is in good agreement with that shown in Fig. 3.

It is seen that the mid-low latitudes are covered by a vast positive band, maximizing at 2.16 (10°N, 100°W), suggesting that the El Nino has reached its climax, with increased 100 hPa height over tropics. There appear two strong negative-value belts, one

(−0.95) located in England and the other (−1.45) in the Aleutians. Also, we see a positive core (1.45) in the northern part of North America with a negative belt to the southeast. Thus, a wavetrain analogous to a PNA pattern emanates from the eastern Pacific, turning to the east and then north into the continent (see the great arc of the figure, a route that agrees well with the result of Fig. 1).

(4) Winter (DJF)

Statistics shows that there are positive values for 217 of the 288 gridpoints, implying that the El Nino event is at the winter phase, with 100 hPa height significantly increased as compared to that of the La Nina year (Fig. 4d). Yet, the decrease in the extratropical Pacific geopotential height gives rise to the enhanced 100 hPa westerly over the Pacific at midlatitudes.

From the foregoing analysis we see that the 100 hPa geopotential height is decreased in spring over the research domain, especially the central Pacific, Iceland and the North Atlantic in the El Nino as opposed to the La Nina year; in summer the height remains low except that it begins to rise in the low-latitude central Pacific; as fall comes, the tropical height positive departure is maintained and expanded westward; the positive anomaly takes place in winter in the southeast of the continent, thus exhibiting a PNA wavetrain.

The lowered 100 hPa height during early days of an El Nino event may serve as an important precursor in diagnosing and predicting the phenomenon. Comparison of winter (DJF) 100 hPa height in the El Nino year with the multi-year mean indicates that negative anomaly occurs at 208 of the 288 points. The details will be published in a separate paper.

V. STATISTICAL DIAGNOSIS AND PREDICTION OF EL NINO EVENT

Forecasting El Nino episodes is a problem of importance and difficulty. It is common practice to determine whether or not the event has happened based on atmospheric circulation and SST anomaly at the burgeoning stage. Therefore, it is necessary to construct a model for more quantitative diagnosis and prognosis of the occurrence in which attempt has been reported in Shi and Cao (1992) and Shi and Luo (1991). The 100 hPa circulation anomaly relative to an El Nino episode has been dealt with in the preceding section. These characteristic quantities, when defined, will be utilized in establishing a model for this purpose and tested to show if they are really associated with the phenomenon. These quantities for spring 100 hPa height mean include:

x_1(30°N, 90 — 70°W); x_2(30°N, 10 — 40°E);
x_3(60°N, 50 — 30°W); x_4(50°N, 60 — 30°W);
x_5(40°N, 110 — 130°E); x_6(10°N,180 — 120°W);
x_7(20°N, 150 — 130°W).

Further, SOI of May and August can be applied for the purpose and as a predictor as well. With the onset years of El Nino and La Nina as given in Table 1 and using data spanning 1956—1990 (35 years) , two diagnosis/prediction schemes are developed in terms of a three-level stepwise discriminant technique. The first takes into account spring/summer data only, leading to the historical fitting of 29/35 with the aid of the established discriminant functions; the second scheme considers spring, summer and autumn data, resulting in the fitting of 31/35. With 1991 and 1992 data as independent samples fed into the model, the year of 1991 (1992) is found to be with the El Nino starting (persisting), suggesting higher ability to deal with the El Nino/La Nina events. Moreover, while an El Nino is developing, 100 hPa atmospheric circulation is already experiencing anomaly. As such, it is necessary to allow for 100 hPa circulation abnormality at its early stage.

VI. CONCLUDING REMARKS

a. In winter northern hemisphere 100 hPa there exists a PNA originating from the tropical central Pacific with its route close to that at 500 hPa level except that the 100 hPa North America part is weaker than the 500 hPa portion. It is found by calculating the 100 hPa centers of action that the 100 hPa PNA IIs show closer correspondence to the El Nino happening than the 500 hPa ones. In the winter when the event is at its peak, 100 hPa displays a vigorous PNA whereas during a La Nina episode an inverse PNA occurs.

b. At the early El Nino stage, 100 hPa low-latitude wind exhibits anomaly that presents itself in tropical central Pacific westerly departures for June — July, which moves into the western Pacific (90—120°E) in September—October. However, intense easterly departures cover 40—50°N at extratropics, which is related to the decreased 100 hPa geopotential height over the Sea of Japan in the fall with an El Nino available.

c. At early El Nino phase, anomaly takes place at the 100 hPa mean circulation. In the spring when the episode begins, the 100 hPa height is lowered on a large scale as compared to the situation of a La Nina year. This can be discerned in the previous winter, too, which is of value to the early diagnosis/prognosis of El Nino events.

The 100 hPa height has a longer record. The interannual variation in the seasonal anomalies can be used to diagnose/predict most El Nino events.

REFERENCES

Arkin P A, 1982. The relationship between interannual variability in the 200 hPa tropical wind field and Southern Oscillation. *Mon. Wea. Rev.*, **110**: 1393—1404.

Chen W Y, 1982. Fluctuation in the Northern Hemisphere 700 mb height field associated with the Southern Oscillation. *Mon. Wea. Rew.*, **110**: 808—823.

Hoskins B J, Karoly D J, 1981. The steady linear response of a spheric atmosphere to thermal and orographic forcing. *J. Atmos. Sci.*, **38**: 1178—1196.

Shi Neng, Cao Hongxing, 1992. A model for three-level discriminant of El Nino disgnosis. *Meteo. Mon.*, **18**: 9—12 (in Chinese).

Shi Neng, Luo Baoliang, 1991. Teleconnection of the 500 hPa polar circulation and El Nino/SO with the temperature field in China. *Adv. Atmos. Sci.*, **3**: 289—298

Shukla J, Wallace J M, 1983. Numerical simulation of the atmospheric response to equatorial sea surface temperature anomalies. *J. Atmos. Sci.*, **40**: 1613—1630.

Wallace J M, Gutzler D S, 1981. Teleconnection in the geopotential height field in the Northern Hemisphere. *Mon. Wea. Rev.*, **109**: 784—812.

Zhu Qianggen, Shi Neng, 1992. Variations in the teleconnection intensity indices and their remote response to the El Nino events in the Northern Hemisphere, *A. M. S.*, **6**: 433—445.